Since January 2020 Elsevier has created a COVID-19 resource centre with free information in English and Mandarin on the novel coronavirus COVID-19. The COVID-19 resource centre is hosted on Elsevier Connect, the company's public news and information website.

Biomedical Signal Processing and Control 71 (2022) 103227

Contents lists available at ScienceDirect

Biomedical Signal Processing and Control

journal homepage: www.elsevier.com/locate/bspc

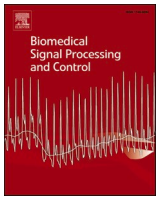

Epidemic model dynamics and fuzzy neural-network optimal control with impulsive traveling and migrating: Case study of COVID-19 vaccination

C. Treesatayapun [a,*]

[a] Department of Robotic and Advanced Manufacturing, CINVESTAV-IPN, Mexico

ARTICLE INFO

Keywords:
COVID-19
Modified SEIAR model
Impulsive migration
Optimal control
Discrete-time systems
Fuzzy rules emulated networks

ABSTRACT

To suppress the epidemics caused by a virus such as COVID-19, three effective strategies listing vaccination, quarantine and medical treatments, are employed under suitable policies. Quarantine motions may affect the economic systems and pharmaceutical medications may be recently in the developing phase. Thus, vaccination seems the best hope of the current situation to control COVID-19 epidemics. In this work, the dynamic model of COVID-19 epidemic is developed when the quarantine factor and the antiviral factor are established as free variables. Moreover, the impulsive populations are comprehended for traveling and migrating of individuals. The proposed dynamics with impulsive distractions are employed to generate the online data. Thereafter, the equivalent model is developed by using only the daily data of symptomatic infectious individuals and the optimal vaccination policy is derived by utilizing the closed-loop control topology. The theoretical framework of the proposed schemes validates the reduction of symptomatic infectious individuals by using fewer doses of vaccines comparing with the scheduling vaccination.

1. Introduction

The COVID-19 epidemic has become a global pandemic rapidly more than other records in the history of RNA viruses outbreaks such as severe acute respiratory syndrome (SARS) in 2002 and middle east respiratory syndrome (MERS) in 2012. At the time this paper has been written, the peak of the third wave is currently observed that has provoked the big wave of economic, civil and health anxieties [1]. By utilizing suitable policies such as vaccination, quarantine and medical treatments, the authority may be able to control the epidemic. Nonetheless, pharmaceutical medications for this coronavirus are still in the developing phase and quarantine may cause the economic issue. In the meantime, the vaccination policy seems to be a worthy option. Unfortunately, the limitation in vaccine production causes an issue because of the high demand [2], especially for the developing countries. Currently, 23.7% of the world population has been fully vaccinated and only 1.3% of people in low-income countries have a chance to get at least one dose of vaccination [3].Therefore, the expansion of sufficient vaccination policy with predicting the epidemic dynamics and minimizing the usage is essential [4,5]. Investigating epidemic dynamics by numerical concept, mathematical models have been formulated by nonlinear ordinary differential equations (ODE) to predict the spread of infectious individuals or to evaluate the defense policies [6,7]. Therefore, the model dynamics can contribute with sufficient information to design the adequate strategies [8,9], especially for the case of COVID-19 when the abundant data can be simply acquired according to the big-data era [10,11]. In general, dynamics of epidemics have been derived under the modifications of SEIR model [12,13] when the individuals have been categorized as follows: Susceptible (S), Exposed (E), Infectious (I) and Recovered (R). It is obvious that the COVID-19 epidemic is an unstable open-loop system with an exponential increase of the infected individuals at the spreading period [14].

Moreover, by considering the epidemic dynamics as the controlled plants, the appropriate defenses i.e. the vaccination policies have been developed such that the next–generation matrix [15], the compensator controller [16], the optimal controller based on fuzzy fractional derivatives [17], the vaccination based on threshold dynamics [18] and the modified sliding mode control [19]. However, those approaches are model based schemes and comprehensive state variables are generally required [20]. From the practical point of view, it's very difficult to monitor and collect all states in real-time according to the continuous-time manner [21,22]. Furthermore, only some states are available at a certain sampling interval [23–25] and the impulsive changes caused by immigration should be considered because the coronavirus can spread

* Corresponding author.
E-mail address: treesatayapun@gmail.com.

https://doi.org/10.1016/j.bspc.2021.103227
Received 11 June 2021; Received in revised form 17 August 2021; Accepted 30 September 2021
Available online 6 October 2021

by the travel and immigrant of people [26,27]. Resulting, the dynamics of epidemic models can be reconsidered as a class of impulsive control systems (ICS) such that [28–30].

ICS schemes have been proposed by some works for a class of discrete-time systems such that [31,32] and linear systems [33]. For the optimal–control problems with ICS, they have a few schemes such as a linear-quadratic (LQ) controller [35], adaptive dynamic programming (ADP) [36] and Pontryagin's maximum principle [26]. For the dynamics with partial knowledge of models, the neural optimal controller [37], the piecewise-constant optimal controller[38], models reducing order [39], neuro-fuzzy inference system [40] and the optimal control based on passivity [41] have been developed with the full state observer and measurement. Moreover, the model dynamics must be well-defined with the appropriate accuracy because of the impulsive data acquisition,[34].

In this work, the conventional SEIR is firstly augmented as the SqvEIAR epidemic model which includes the quarantined individuals and subgroups of ineffectively vaccinated and effectively vaccinated individuals. Thus, general dynamics of SqvEIAR are formulated as a class of discrete-time impulsive control systems when the vaccination policy is represented as the control effort. Secondly, the equivalent model is established by an adaptive network called fuzzy rules emulated network (FREN) on the impulsive axis. The learning law is utilized to improve the model's performance with the convergent analysis of internal signals. Finally, the optimal vaccination policy is derived by using only the data of symptomatic infectious (I) on the impulsive axis when the impulsive disturbances of susceptible (S), exposed (E), symptomatic infectious (I) and asymptomatic infectious (A) individuals are consolidated to mimic impulsive traveling and migrating. The analysis of closed-loop performance is conducted by the Lyapunov method with the extension of negative control–direction.

The main contributions of this paper are briefly expressed as the followings:

- Unlike SEIR and its modifications in [26,28,30], the vaccination is directly employed as the impulsive control input by the proposed SqvEIAR dynamics. Therefore, the equivalent model and the controller are derived according to the impulsive traveling and migrating of individuals.
- By utilizing only the daily data of symptomatic infectious individuals (I) on the impulsive axis, the equivalent model is established and the full state observer, which is generally required such as the works in [22,24,26], is completely omitted here.
- The controlled system of SqvEIAR dynamics on the impulsive axis is negative control direction by nature. The proposed controller is directly designed for this case when the closed-loop performance is guaranteed.

The rest of this paper is organized as follows. Section 2 introduces the SqvEIAR dynamics and problem formulation according to the controlled system with vaccination policy. In Section 3, the equivalent model is established by utilizing an adaptive network FREN and the daily data of symptomatic infectious individuals. The optimal vaccination policy is derived in Section 4 with the performance analysis. Numerical systems and comparison results are provided in Section 5 to validate the proposed scheme. Finally, conclusions and future works are given in Section 6.

2. Mathematical model and problem formulation

In this section, a mathematical model called SqvEIAR is attained by integrating state variables of quarantined people and vaccinated individuals with the standard SEIAR. Thereafter, some problems with the impulsive iteration and sampling for the monitoring of symptomatic infectious individuals are clarified.

2.1. Model of SqvEIAR epidemic

A flow diagram of SqvEIAR model is depicted in Fig. 1. In this model, the total population is divided into nine groups, i.e. susceptible $S(t)$, exposed $E(t)$, symptomatic infectious $I(t)$, asymptomatic infectious $A(t)$, recovered $R(t)$, ineffectively vaccinated $V^i(t)$, effectively vaccinated but still unprotected $V(t)$, protected $P(t)$ and quarantined $Q(t)$ individuals. Thus, the dynamic system of SqvEIAR is derived as follows:

$$\begin{aligned}
\dot{S}(t) &= -\beta\Lambda(t)S(t) - \left[\lambda + \upsilon(t)\right]S(t),\\
\dot{Q}(t) &= \lambda S(t),\\
\dot{V}^i(t) &= (1-e)\upsilon(t)S(t) - \beta\Lambda(t)V^i(t),\\
\dot{V}(t) &= e\upsilon(t)S(t) - \beta\Lambda(t)V(t) - \omega V(t),\\
\dot{E}(t) &= \beta\Lambda(t)\left[S(t) + V(t) + V^i(t)\right] - \mathfrak{f}E(t),\\
\dot{I}(t) &= p\mathfrak{f}E(t) - \left[\mathfrak{a} + \mathfrak{r}\right]I(t) + (1-z)\mathfrak{n}A(t),\\
\dot{A}(t) &= (1-p)\mathfrak{f}E(t) - \mathfrak{n}A(t),\\
\dot{R}(t) &= z\mathfrak{n}A(t) + \mathfrak{f}\left[\mathfrak{a} + \mathfrak{r}\right]I(t),\\
\dot{P}(t) &= \omega V(t),
\end{aligned} \tag{1}$$

where

$$\Lambda(t) = \epsilon_L E(t) + [1-q_L]I(t) + d_L A(t), \tag{2}$$

and all parameters are described by Table 1. From the control engineering point of view, in this work, the control input is assigned as the vaccination policy $\upsilon(t)$ and the output is the number of symptomatic infectious individuals $I(t)$. Then, the controlled system under our investigation is conceptually rewritten as

$$\dot{I}(t) = F_c\left(\upsilon(t), I(t), \Xi(t)\right), \tag{3}$$

where $F_c(-)$ is an unknown function and $\Xi(t)$ denotes other states such that $S(t), Q(t), V^i(t), V(t), E(t), A(t)$ and $R(t)$. Theoretically, the system in (3) is discretized by Euler approximation with the sampling time T_s as

$$\begin{aligned}
I(k+1) = &\ T_s F_c(\upsilon(k), I(k), \Xi(k)) + I(k),\\
= &\ F_d(\upsilon(k), I(k), \Xi(k)),
\end{aligned} \tag{4}$$

where k is the sampling–index and $F_d(-)$ is the unknown nonlinear function. It's worth to emphasize that $F_d(-)$ in (4) is not precisely required to design a model-free controller. Furthermore, in this work, only the relation between the input $\upsilon(k)$ and the output $I(k+1)$ is obliged by the format of IF-THEN rules.

Fig. 2 illustrates the concept of SqvEIAR dynamics as the controlled plant mentioned above. By utilizing impulsive sampling interval κ and the first sampling–index κ_j of the j^{th} day as the block diagram in Fig. 2, the vaccination policy $\upsilon(k)$ is attended in the impulsive axis as

$$\upsilon(k) = \begin{cases} 0 & \text{if} k \neq \kappa_j,\\ \upsilon(\kappa_j) & \text{otherwise.} \end{cases} \tag{5}$$

Therefore, it's clear that the output $I(\kappa_j)$ can be rewritten as the function of $\upsilon(\kappa_j)$ such that

$$I(k) = \begin{cases} F_d(I(k-1), \Xi(k-1)) & \text{if} k \neq \kappa_j,\\ F_d(I_{k-1}) + G_u(\upsilon(\kappa_j)) & \text{otherwise.} \end{cases} \tag{6}$$

where $G_u(-)$ denotes the unknown function which makes a change of $I(k)$ caused by the impulsive input or the vaccination policy $\upsilon(\kappa_j)$.

2.2. A class of impulsive controlled plants

By considering SqvEIAR dynamics as the controlled plant in Fig. 2 at the impulsive index $k = \kappa_j$, the input $u(\kappa_j)$ is the vaccination policy $\upsilon(\kappa_j)$ and the output state $x(\kappa_j)$ is the number of infected individuals $I(\kappa_j)$.

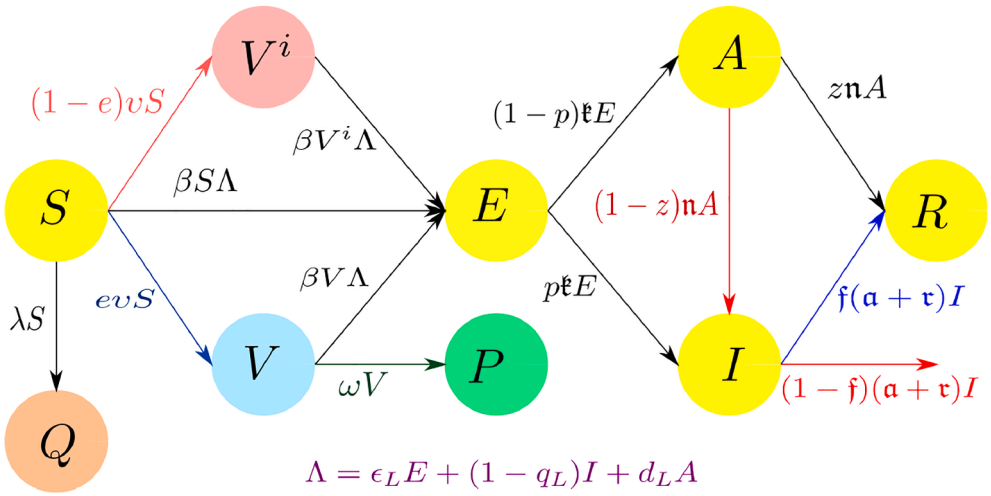

Fig. 1. Flow diagram of the proposed SqvEIAR epidemic model.

Table 1
Descriptions Model's parameters.

Parameter	Description	Remark
β	Transmission rate	According to the initial population
e	Vaccine efficacy	Average efficacy
ω	Progressive rate	Protected group
$\mathfrak{f}$	Progressive rate	Infected group
p	Fraction	Exposed group
$\mathfrak{r}$	Recovery rate	Infected group
$\mathfrak{a}$	Antiviral factor	Antiviral therapies
$\mathfrak{f}$	Fraction	Infected group
$\mathfrak{n}$	Recovery rate	Asymptomatic group
z	Fraction	Asymptomatic group
λ	Quarantine rate	Approximated policy [0,1)
ϵ_L	Infectivity reduction	$\Lambda(t)$:Exposed group
q_L	Infectivity facto	$\Lambda(t)$:Infected group
d_L	Infectivity reduction	$\Lambda(t)$:Asymptomatic group

Thus, the system dynamics (6) can be represented as

$$\begin{aligned} x(k) &= F_d \circ F_d \circ \cdots F_d\left(x(\kappa_{j-1}+1)\right), \\ &= F_d^{n_j}\left(x(\kappa_{j-1}+1)\right), \end{aligned} \tag{7}$$

where n_j is the number of sampling intervals during κ_{j-1} to κ_j. By using one step-back of (7), it leads to

$$x(k-1) = F_d^{n_j}\left(x(\kappa_{j-1})\right). \tag{8}$$

Recalling (6), when $k = \kappa_j$, the dynamics (7) can be obtained as

$$x(\kappa_j) = F_d(x_{k-1}) + G_u(u(\kappa_j)). \tag{9}$$

By substitute x_{k-1} from (8) into (9), it yields

$$\begin{aligned} x(\kappa_j) &= F_d\left(F_d^{n_j}\left(x(\kappa_{j-1})\right)\right) + G_u(u(\kappa_j)), \\ &= F_T\left(x(\kappa_{j-1}), u(\kappa_j)\right), \end{aligned} \tag{10}$$

where $F_T(-)$ is the unknown function that represents the dynamics of the controlled plant on the impulsive axis.

Without loss of generality, our problem formulation can be concluded that founding the control policy $u(\kappa_j)$ when the function $F_T(-)$ is unknown and $x(\kappa_j), j = 1, 2, \ldots$ is only the measurable state.

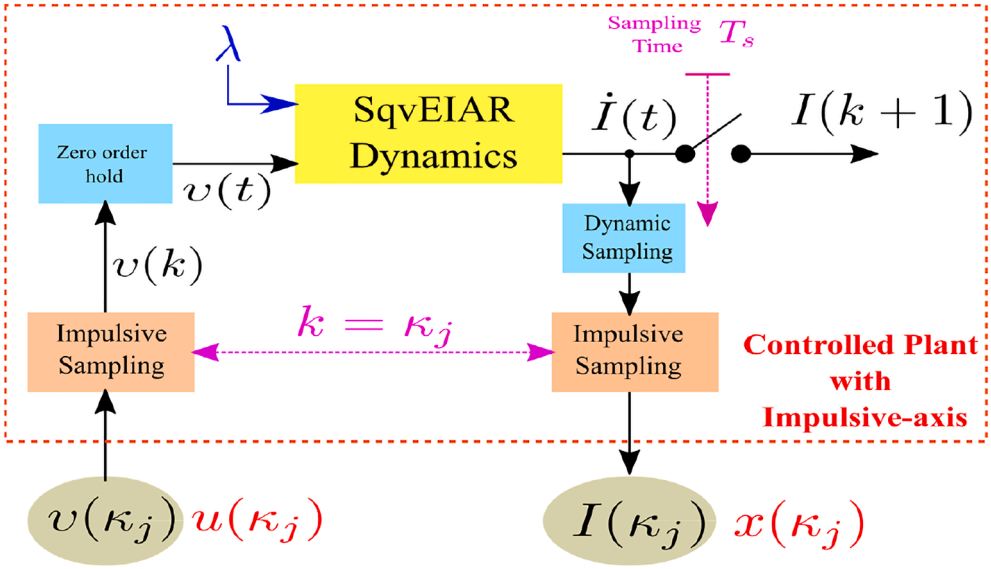

Fig. 2. SqvEIAR on Impulsive-axis.

Remark 1. It worth to note that the unknown function $F_T(-)$ is only dependent on the state at κ_{j-1} and the control effort at κ_j. Unlike the works on impulsive systems such as [37,32,35], the equivalent model developed in this work is required only the state at the previous impulsive axis and the current control effort. That will reduce the number or sampling data.

3. Equivalent model with impulsive sampling

3.1. Equivalent model based on FREN

By employing the dynamic-linearization [44,45] with the unknown function $F_T(-)$ in (10), there exist functions $f_T(x(\kappa_{j-1}))$ and $g_T(x(\kappa_{j-1}))$ for the affine dynamics such that

$$x(\kappa_j) = f_T\left(x(\kappa_{j-1})\right) + g_T\left(x(\kappa_{j-1})\right)u(\kappa_j). \tag{11}$$

Furthermore, by utilizing the results in [46] with dynamics (1)–(4), we have

$$|f_T\left(x(\kappa_{j-1})\right)| \leqslant \alpha_f |x(\kappa_{j-1})|, \tag{12}$$

and

$$|g_T\left(x(\kappa_{j-1})\right)| \leqslant \alpha_g |x(\kappa_{j-1})|, \tag{13}$$

where α_f and α_s are positive constants. It's worth clarifying that the parameter α_f characterizes virus states such that $\alpha_f < 1$ and $\alpha_f > 1$ according to the virus at decreasing and increasing phases, respectively. The parameter α_g represents the control gain $g_T(-)$ in (11). Furthermore, both parameters α_f and α_g are unknown and only their existence is required for further analysis.

For the unknown affine dynamics (11), the equivalent model based on FREN can by established as

$$\hat{x}(\kappa_j) = f_m\left(x(\kappa_{j-1})\right) + g_m\left(x(\kappa_{j-1})\right)u(\kappa_j), \tag{14}$$

where $\hat{x}(\kappa_j)$ is the estimated state. Functions $f_m(x(\kappa_{j-1}))$ and $g_m(x(\kappa_{j-1}))$ are derived by FREN's computation as

$$f_m\left(x\left(\kappa_{j-1}\right)\right) = \beta_f^T\left(\kappa_{j-1}\right)\phi\left(\kappa_{j-1}\right), \tag{15}$$

and

$$g_m\left(x\left(\kappa_{j-1}\right)\right) = \beta_g^T\left(\kappa_{j-1}\right)\phi\left(\kappa_{j-1}\right), \tag{16}$$

respectively, where $\phi(\kappa_{j-1})$ is the membership vector of $x(\kappa_{j-1})$ and $\beta_f(\kappa_{j-1})$ and $\beta_g(\kappa_{j-1})$ are adjustable parameters.

By utilizing (15) and (16), the network architecture is established in Fig. 3 where N denotes as the number of IF-THEN rules such that:

IF $x(\kappa_{j-1})$ is Small (μ_1) THEN $f_m(x(\kappa_{j-1}))$ should be Small and $g_m(x(\kappa_{j-1}))$ should be Small.

Thereafter, the learning laws are derived to tune all adjustable parameters $\beta_{f,g}(\kappa_j)$ with the estimation error $\hat{e}(\kappa_j)$ defined by

$$\hat{e}(\kappa_j) = x(\kappa_j) - \hat{x}(\kappa_j). \tag{17}$$

It's worth remaking that $x(\kappa_j)$ is stationary during κ_j to κ_{j+1}^-. Resulting, the estimation error in (17) is rewritten according to the i^{th} inner iteration as

$$\hat{e}(\kappa_j, i+1) = x(\kappa_j) - \hat{x}(\kappa_j, i+1), \tag{18}$$

where

$$\hat{x}\left(\kappa_j, i+1\right) = \beta_f^T\left(\kappa_{j-1}, i\right)\phi\left(\kappa_{j-1}, i\right) + \beta_g^T\left(\kappa_{j-1}, i\right)\phi\left(\kappa_{j-1}, i\right)u\left(\kappa_j\right), \tag{19}$$

$\forall i = 0, 1, 2, \cdots, i_{max}$ and $\hat{x}(\kappa_j, 1)$ is the first estimated state at $k = \kappa_j$ before initiating the inner iterative learning law.

Let's define the cost function $\hat{E}(\kappa_j, i+1)$ over the i^{th}-iteration as

$$\hat{E}\left(\kappa_j, i+1\right) = \frac{1}{2}\hat{e}^2\left(\kappa_j, i+1\right). \tag{20}$$

Employing the gradient search, the learning law of $\beta_f(\kappa_{j-1}, i)$ is obtained as

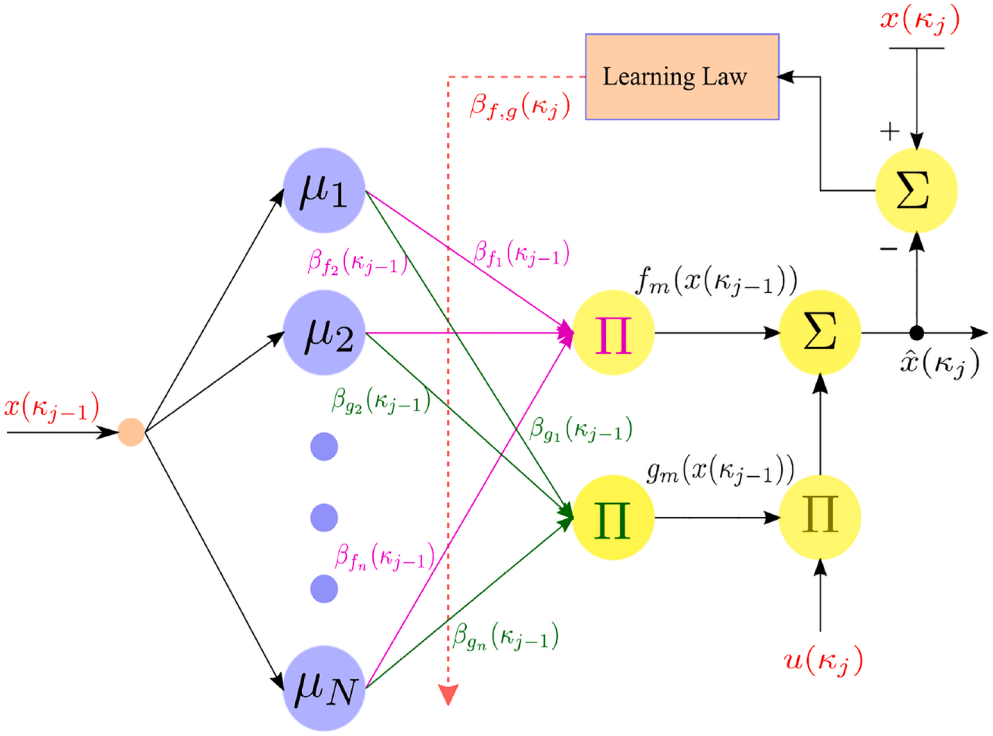

Fig. 3. FREN: Equivalent model.

$$\beta_f\left(\kappa_{j-1}, i+1\right) = \beta_f\left(\kappa_{j-1}, i\right) - \eta_f \frac{\partial \widehat{E}\left(\kappa_j, i+1\right)}{\partial \beta_f\left(\kappa_{j-1}, i\right)}, \tag{21}$$

where a positive constant η_f is the learning rate. By utilizing the chain rule according to (18) and (20), we have

$$\begin{aligned} \frac{\partial \widehat{E}\left(\kappa_j, i+1\right)}{\partial \beta_f\left(\kappa_{j-1}, i\right)} &= \frac{\partial \widehat{E}\left(\kappa_j, i+1\right)}{\partial \widehat{e}\left(\kappa_j, i+1\right)} \frac{\partial \widehat{e}\left(\kappa_j, i+1\right)}{\partial \widehat{x}\left(\kappa_j, i+1\right)} \frac{\partial \widehat{x}\left(\kappa_j, i+1\right)}{\partial \beta_f\left(\kappa_{j-1}, i\right)}, \\ &= -\widehat{e}\left(\kappa_j, i+1\right)\phi\left(\kappa_{j-1}, i\right). \end{aligned} \tag{22}$$

Substitution (22) into (21), the learning law for $\beta_f(\kappa_{j-1}, i)$ is obtained as

$$\beta_f\left(\kappa_{j-1}, i+1\right) = \beta_f\left(\kappa_{j-1}, i\right) + \eta_f \widehat{e}\left(\kappa_j, i+1\right)\phi\left(\kappa_{j-1}, i\right). \tag{23}$$

By repeating the similar procedure with (21)–(23) with $\beta_g(-)$, we have

$$\beta_g\left(\kappa_{j-1}, i+1\right) = \beta_g\left(\kappa_{j-1}, i\right) - \eta_g \frac{\partial \widehat{E}\left(\kappa_j, i+1\right)}{\partial \beta_g\left(\kappa_{j-1}, i\right)}, \tag{24}$$

where η_g is the learning rate. By utilizing the chain rule again, it yields to

$$\begin{aligned} \frac{\partial \widehat{E}\left(\kappa_j, i+1\right)}{\partial \beta_g\left(\kappa_{j-1}, i\right)} &= \frac{\partial \widehat{E}\left(\kappa_j, i+1\right)}{\partial \widehat{e}\left(\kappa_j, i+1\right)} \frac{\partial \widehat{e}\left(\kappa_j, i+1\right)}{\partial \widehat{x}\left(\kappa_j, i+1\right)} \frac{\partial \widehat{x}\left(\kappa_j, i+1\right)}{\partial \beta_g\left(\kappa_{j-1}, i\right)}, \\ &= -\widehat{e}\left(\kappa_j, i+1\right)\phi\left(\kappa_{j-1}, i\right)u\left(\kappa_j\right). \end{aligned} \tag{25}$$

Thus, the learning law for $\beta_g(\kappa_{j-1}, i)$ is derived as

$$\beta_g\left(\kappa_{j-1}, i+1\right) = \beta_g\left(\kappa_{j-1}, i\right) + \eta_g \widehat{e}\left(\kappa_j, i+1\right)u\left(\kappa_j\right)\phi\left(\kappa_{j-1}, i\right). \tag{26}$$

To terminate the inner iteration, two conditions are employed as *i*: the maximum iteration number $i \geqslant i_{max}$ and *ii*: the limited estimation error $\left|\widehat{e}\left(\kappa_j, i+1\right)\right| \leqslant \varepsilon_o$, where ε_o is a designed parameter.

3.2. Model performance analysis

In general, the performance of learning laws developed under the gradient search is obviously related to the setting of learning rates. The following theorem is employed to select the learning rates η_f and η_g with the convergence of the estimation error.

Theorem 3.1. For a class of impulsive system dynamics (14), the estimation error (17) of the equivalent model based on FREN (14) is a convergent sequence along with the iteration axis when the learning rates η_f and η_g are selected by the following conditions:

$$0 \leqslant \eta_f < \frac{\gamma_f}{\phi_M}, \tag{27}$$

and

$$0 \leqslant \eta_g < \frac{\gamma_g}{u_M^2 \phi_M}, \tag{28}$$

where $0 < \gamma_f < 1, 0 < \gamma_g < 1, u_M = \max\left|u(\kappa_j)\right|, \forall j$ and $\phi_M = \sup_{\forall x}\{\left|\left|\phi(x)\right|\right|^2\}$.

Proof. By recalling the universal function approximation of FREN in [42], it exists the ideal parameters $\beta_f^*(\kappa_{j-1})$ and $\beta_g^*(\kappa_{j-1})$ such that

$$x\left(\kappa_j\right) = \beta_f^{*T}\left(\kappa_{j-1}\right)\phi\left(\kappa_{j-1}, i\right) + \beta_g^{*T}\left(\kappa_{j-1}\right)\phi\left(\kappa_{j-1}, i\right)u\left(\kappa_j\right) + \varepsilon_s\left(k\right), \tag{29}$$

where $\varepsilon_s(k)$ is a bounded residue error. During the inner iteration i^{th}, $\phi(\kappa_{j-1}, i)$ is fixed, thus, the relation in (29) can be rewritten as

$$x\left(\kappa_j\right) = \beta_f^{*T}\left(\kappa_{j-1}\right)\phi\left(\kappa_{j-1}\right) + \beta_g^{*T}\left(\kappa_{j-1}\right)\phi\left(\kappa_{j-1}\right)u\left(\kappa_j\right) + \varepsilon_s\left(k\right), \tag{30}$$

By using (29) with (14–16), we have

$$\begin{aligned} \widehat{e}\left(\kappa_j, i+1\right) &= x\left(\kappa_j\right) - \widehat{x}\left(\kappa_j, i+1\right), \\ &= \beta_f^{*T}\left(\kappa_{j-1}\right)\phi\left(\kappa_{j-1}\right) + \beta_g^{*T}\left(\kappa_{j-1}\right)\phi\left(\kappa_{j-1}\right)u\left(\kappa_j\right) + \varepsilon_s\left(k\right) - \beta_f^{T}\left(\kappa_{j-1}, i\right)\phi\left(\kappa_{j-1}\right) - \beta_g^{T}\left(\kappa_{j-1}, i\right)\phi\left(\kappa_{j-1}\right)u\left(\kappa_j\right), \\ &= \widetilde{\beta}_f^{T}\left(\kappa_{j-1}, i\right)\phi\left(\kappa_{j-1}\right) + \widetilde{\beta}_g^{T}\left(\kappa_{j-1}, i\right)\phi\left(\kappa_{j-1}\right)u\left(\kappa_j\right) + \varepsilon_s\left(k\right), \end{aligned} \tag{31}$$

where

$$\widetilde{\beta}_f^{T}\left(\kappa_{j-1}, i\right) = \beta_f^{*}\left(\kappa_{j-1}\right) - \beta_f\left(\kappa_{j-1}, i\right), \tag{32}$$

and

$$\widetilde{\beta}_g^{T}\left(\kappa_{j-1}, i\right) = \beta_g^{*}\left(\kappa_{j-1}\right) - \beta_g\left(\kappa_{j-1}, i\right). \tag{33}$$

With one step back on i^{th} iteration, the learning laws in (23) and (26) can be rearranged as

$$\beta_f\left(\kappa_{j-1}, i\right) = \beta_f\left(\kappa_{j-1}, i-1\right) + \eta_f \widehat{e}\left(\kappa_j, i\right)\phi\left(\kappa_{j-1}\right), \tag{34}$$

and

$$\beta_g\left(\kappa_{j-1}, i\right) = \beta_g\left(\kappa_{j-1}, i-1\right) + \eta_g \widehat{e}\left(\kappa_j, i\right)u\left(\kappa_j\right)\phi\left(\kappa_{j-1}\right), \tag{35}$$

respectively. By applying (34) and (35) with (32) and (33), respectively, we obtain

$$\begin{aligned} \widetilde{\beta}_f^{T}\left(\kappa_{j-1}, i\right) &= \beta_f^{*}\left(\kappa_{j-1}\right) - \beta_f\left(\kappa_{j-1}, i-1\right) - \eta_f \widehat{e}\left(\kappa_j, i\right)\phi\left(\kappa_{j-1}\right), \\ &= \widetilde{\beta}_f^{T}\left(\kappa_{j-1}, i-1\right) - \eta_f \widehat{e}\left(\kappa_j, i\right)\phi\left(\kappa_{j-1}\right), \end{aligned} \tag{36}$$

and

$$\begin{aligned} \widetilde{\beta}_g^{T}\left(\kappa_{j-1}, i\right) &= \beta_g^{*}\left(\kappa_{j-1}\right) - \beta_g\left(\kappa_{j-1}, i-1\right) - \eta_g \widehat{e}\left(\kappa_j, i\right)u\left(\kappa_j\right)\phi\left(\kappa_{j-1}\right), \\ &= \widetilde{\beta}_g^{T}\left(\kappa_{j-1}, i-1\right) - \eta_g \widehat{e}\left(\kappa_j, i\right)u\left(\kappa_j\right)\phi\left(\kappa_{j-1}\right). \end{aligned} \tag{37}$$

By substituting (36) and (37) into (31), it leads to

$$\begin{aligned}\widehat{e}(\kappa_j,i+1) &= \left[\widetilde{\beta}_f\left(\kappa_{j-1},i-1\right)-\eta_f\widehat{e}\left(\kappa_j,i\right)\phi\left(\kappa_{j-1}\right)\right]^T\phi\left(\kappa_{j-1}\right)+\left[\widetilde{\beta}_g\left(\kappa_{j-1},i-1\right)-\eta_g\widehat{e}\left(\kappa_j,i\right)u\left(\kappa_j\right)\phi\left(\kappa_{j-1}\right)\right]^T\phi\left(\kappa_{j-1}\right)u\left(\kappa_j\right)+\varepsilon_s\left(k\right),\\ &= \widetilde{\beta}_f^T\left(\kappa_{j-1},i-1\right)\phi\left(\kappa_{j-1}\right)+\widetilde{\beta}_g^T\left(\kappa_{j-1},i-1\right)\phi\left(\kappa_{j-1}\right)u\left(\kappa_j\right)-\eta_f\widehat{e}\left(\kappa_j,i\right)\left|\left|\phi\left(\kappa_{j-1}\right)\right|\right|^2-\eta_g\widehat{e}\left(\kappa_j,i\right)u^2\left(\kappa_j\right)\left|\left|\phi\left(\kappa_{j-1}\right)\right|\right|^2+\varepsilon_s\left(k\right),\\ &= \widehat{e}\left(\kappa_j,i\right)-\eta_f\widehat{e}\left(\kappa_j,i\right)\left|\left|\phi\left(\kappa_{j-1}\right)\right|\right|^2-\eta_g\widehat{e}\left(\kappa_j,i\right)u^2\left(\kappa_j\right)\left|\left|\phi\left(\kappa_{j-1}\right)\right|\right|^2,\\ &= \left[1-\eta_f\left|\left|\phi\left(\kappa_{j-1}\right)\right|\right|^2-\eta_g u^2\left(\kappa_j\right)\left|\left|\phi\left(\kappa_{j-1}\right)\right|\right|^2\right]\widehat{e}\left(\kappa_j,i\right).\end{aligned} \tag{38}$$

To simplify, let's define

$$\mathfrak{N}\left(\kappa_j\right)=1-\eta_f||\phi\left(\kappa_{j-1}\right)||^2-\eta_g u^2\left(\kappa_j\right)||\phi\left(\kappa_{j-1}\right)||^2. \tag{39}$$

Thus, the estimation error along the i-iteration can be simplified as

$$\widehat{e}\left(\kappa_j,i+1\right)=\mathfrak{N}\left(\kappa_j\right)\widehat{e}\left(\kappa_j,i\right). \tag{40}$$

Recalling the conditions in (27) and (28), it's clear that

$$|\mathfrak{N}\left(\kappa_j\right)|\leqslant|1-\frac{\gamma_f}{\phi_M}||\phi\left(\kappa_{j-1}\right)||^2-\frac{\gamma_g}{u_M^2\phi_M}u^2\left(\kappa_j\right)||\phi\left(\kappa_{j-1}\right)||^2|<1. \tag{41}$$

Thus, it can be concluded that the estimation error $\widehat{e}(\kappa_j,i)$ is a convergent sequence on the i-iteration axis with the proposed learning algorithm. The proof is completed. It's worth noting that the estimated functions $f_m(\boldsymbol{x}(\kappa_{j-1}))$ and $g_m(\boldsymbol{x}(\kappa_{j-1}))$ in (15) and (16) are bounded such that

$$0^2\leqslant f_m^{min}\leqslant|f_m\left(x\left(\kappa_{j-1}\right)\right)|\leqslant f_m^{max}, \tag{42}$$

and

$$0<g_m^{min}\leqslant|g_m\left(x\left(\kappa_{j-1}\right)\right)|\leqslant g_m^{max}, \tag{43}$$

$\forall j=1,2,\cdots$, according to the result from Theorem 3.1 and FREN's property [42,43].

Remark 2. For the controllable systems, it's required that $\left|g_m(\boldsymbol{x}(\kappa_{j-1}))\right|\neq 0$. This is one of our advantages of the proposed equivalent model when the condition in (43) is always satisfied. Furthermore, the evidence will be demonstrated in the section on numerical results.

4. Impulsive optimal controller for vaccination policy

In this section, the optimal vaccination policy for SqvEIAR dynamics is derived on the impulsive axis. To simplify, the impulsive index κ_j in (10) is solely noted as j. Thus, the controlled plant (10) can be simply rewritten as

$$x(j)=F_T(x(j-1),u(j)), \tag{44}$$

and the equivalent model in (14) can be also simplified as

$$\widehat{x}(j)=f_m(x(j-1))+g_m(x(j-1))u(j). \tag{45}$$

Let's define the unity function $r(j)$ as

$$r\left(j\right)=\gamma_x x^2\left(j-1\right)+\gamma_u u^2\left(j\right), \tag{46}$$

where γ_x and γ_u are positive constants. Thereafter, the long term cost function $J(j)$ is given as

$$\begin{aligned}J(j) &= r(j)+\gamma r(j+1)+\gamma^2 r\left(j+2\right)+\gamma^3 r\left(j+3\right)+\cdots,\\ &= r(j)+\gamma J(j+1),\end{aligned} \tag{47}$$

where $0<\gamma<1$ is a discount factor. The optimal solution can be obtained when $\frac{\partial J(j)}{\partial u(j)}=0$. By using (46) and (47), it yields

$$\begin{aligned}\frac{\partial J(j)}{\partial u(j)} &= \frac{\partial r(j)}{\partial u(j)}+\gamma\frac{\partial J(j+1)}{\partial u(j)},\\ &= 2\gamma_u u\left(j\right)+\gamma\left[\frac{\partial J(j+1)}{\partial r(j+1)}\frac{\partial r(j+1)}{\partial x(j)}\frac{\partial x(j)}{\partial u(j)}\right],\\ &= 2\gamma_u u\left(j\right)+\gamma\left[2\gamma_x x\left(j\right)\frac{\partial x(j)}{\partial u(j)}\right].\end{aligned} \tag{48}$$

By setting $\frac{\partial J(j)}{\partial u(j)}=0$, the ideal-optimal control law $u^*(j)$ is derived as

$$u^*\left(j\right)=-\gamma\frac{\gamma_x}{\gamma_u}x\left(j\right)\frac{\partial x(j)}{\partial u(j)}. \tag{49}$$

When the function $F_T(-)$ in (44) is unknown, It's obvious that $\frac{\partial x(j)}{\partial u(j)}$ can not be determined directly because of the unknown function $F_T(-)$ in (44). Furthermore, the relation of $x(j)$ with respect to $u(j)$ also leads to the causality problem according to the diagram in Fig. 2.

To utilize the control law based on (48) and (49), the equivalent model (45) is employed as $x(j)\rightarrow\widehat{x}(j)$. By recalling (45), it leads to

$$\frac{\partial x(j)}{\partial u(j)}\approx\frac{\partial\widehat{x}(j)}{\partial u(j)}=g_m\left(x\left(j-1\right)\right). \tag{50}$$

Thus, the relation in (48) can be rearranged as

$$\begin{aligned}\frac{\partial J(j)}{\partial u(j)} &\doteq 2\gamma_u u(j)+\gamma[2\gamma_x[f_m(x(j-1))+g_m(x(j-1))u(j)]g_m(x(j-1))],\\ &= 2\left\{\left[\gamma_u+\gamma\gamma_x g_m^2\left(x_{j-1}\right)\right]u\left(j\right)+\gamma\gamma_x g_m\left(x_{j-1}\right)f_m\left(x_{j-1}\right)\right\}.\end{aligned} \tag{51}$$

By setting $\frac{\partial J(j)}{\partial u(j)}=0$, thus, the control law is obtained as

$$u\left(j\right)=-\frac{\gamma\gamma_x g_m\left(x_{j-1}\right)}{\gamma_u+\gamma\gamma_x g_m^2\left(x_{j-1}\right)}f_m\left(x_{j-1}\right). \tag{52}$$

It's clear that the proposed control law in (52) is a model free controller utilizing under the estimated functions $f_m(-)$ and $g_m(-)$ from FREN. Furthermore, only the data of infected individuals on the impulsive axis $x(j)\doteq I(\kappa_j)$ is required. Unlike the works in [26,41], the full-state observers are strictly demanded at all sampling intervals k as real-time monitoring.

Therefore, the closed–loop performance is guaranteed by employing the Lyapunov method and and algebraic inequality procedures as the following theorem.

Theorem 4.1. *By utilizing the vaccination policy $v(\kappa_j)$ on the impulsive axis via the control law (52) for the SqvEIAR dynamics in (1), the closed-loop performance is guaranteed under the number of infected individuals when the designed parameters are given as the following conditions:*

i: *γ_u in (46) is defined as a time varying parameter $\gamma_u(j-1)$ such that*

$$\gamma_u\left(j-1\right)=\alpha_u g_m^2\left(x_{j-1}\right), \tag{53}$$

where α_u is a positive constant and

ii: *γ_x and γ in (46) and (47), respectively, are satisfied*

$$\frac{\gamma\gamma_x}{\alpha_u+\gamma\gamma_x}\leqslant\frac{1-\alpha_f}{\alpha_g}\frac{g_m^{min}}{f_m^{max}}. \tag{54}$$

Proof. By employing the control law (52) with the dynamics (11), it yields

$$x\left(j\right)=f_T\left(x_{j-1}\right)-\frac{\gamma\gamma_x g_m\left(x_{j-1}\right)g_T\left(x_{j-1}\right)}{\gamma_u+\gamma\gamma_x g_m^2\left(x_{j-1}\right)}f_m\left(x_{j-1}\right). \tag{55}$$

Let's define the Lyapunov candidate function $L(j)$ as

$$L(j)=|x(j)|. \tag{56}$$

Thus, the change of (56) can be obtained as

$$\begin{aligned}\Delta L(j)=&\ L(j)-L(j-1),\\ =&\ |x(j)|-|x(j-1)|,\\ =&\ \left|f_T\left(x_{j-1}\right)-\frac{\gamma\gamma_x g_m\left(x_{j-1}\right)g_T\left(x_{j-1}\right)}{\gamma_u+\gamma\gamma_x g_m^2\left(x_{j-1}\right)}f_m\left(x_{j-1}\right)\right|-\left|x\left(j-1\right)\right|,\\ =&\ \left|f_T\left(x_{j-1}\right)-\gamma_o\left(x_{j-1}\right)f_m\left(x_{j-1}\right)g_T\left(x_{j-1}\right)\right|-\left|x(j-1)\right|,\\ \leqslant&\ \left|f_T\left(x_{j-1}\right)\right|+\left|\gamma_o\left(x_{j-1}\right)f_m\left(x_{j-1}\right)\right|\left|g_T\left(x_{j-1}\right)\right|-\left|x(j-1)\right|,\end{aligned} \tag{57}$$

where

$$\gamma_o\left(x_{j-1}\right)=\frac{\gamma\gamma_x g_m\left(x_{j-1}\right)}{\gamma_u+\gamma\gamma_x g_m^2\left(x_{j-1}\right)}. \tag{58}$$

Recalling (12) and (13), we have

$$\begin{aligned}\Delta L(j)\leqslant&\ \alpha_f\left|x(j-1)\right|+\left|\gamma_o\left(x_{j-1}\right)f_m\left(x_{j-1}\right)\right|\alpha_g\left|x(j-1)\right|-\left|x(j-1)\right|,\\ \leqslant&\ \left[\alpha_f+\alpha_g\left|\gamma_o\left(x_{j-1}\right)f_m\left(x_{j-1}\right)\right|-1\right]\left|x(j-1)\right|.\end{aligned} \tag{59}$$

In order to obtain $\Delta L(j)\leq 0$, it's required that

$$\alpha_f+\alpha_g\left|\gamma_o\left(x_{j-1}\right)f_m\left(x_{j-1}\right)\right|\leq 1, \tag{60}$$

or

$$\left|\gamma_o\left(x_{j-1}\right)f_m\left(x_{j-1}\right)\right|\leqslant\frac{1-\alpha_f}{\alpha_g}. \tag{61}$$

By using $\gamma_o(x_{j-1})$ (58) and γ_u in (53), it yields

$$\begin{aligned}\left|\frac{\gamma\gamma_x g_m\left(x_{j-1}\right)}{\gamma_u+\gamma\gamma_x g_m^2\left(x_{j-1}\right)}f_m\left(x_{j-1}\right)\right|\leqslant&\ \frac{1-\alpha_f}{\alpha_g},\\ \left|\frac{\gamma\gamma_x g_m\left(x_{j-1}\right)}{\alpha_u g_m^2\left(x_{j-1}\right)+\gamma\gamma_x g_m^2\left(x_{j-1}\right)}f_m\left(x_{j-1}\right)\right|\leqslant&\ \frac{1-\alpha_f}{\alpha_g},\\ \left|\frac{\gamma\gamma_x}{\alpha_u+\gamma\gamma_x}\frac{f_m\left(x_{j-1}\right)}{g_m\left(x_{j-1}\right)}\right|\leqslant&\ \frac{1-\alpha_f}{\alpha_g}.\end{aligned} \tag{62}$$

The designed parameters γ,γ_x and α_u are positive constants, thus, the relation in (62) can be rearranged as

$$\frac{\gamma\gamma_x}{\alpha_u+\gamma\gamma_x}\leqslant\frac{1-\alpha_f}{\alpha_g}\left|\frac{g_m\left(x_{j-1}\right)}{f_m\left(x_{j-1}\right)}\right|, \tag{63}$$

or

$$\frac{\gamma\gamma_x}{\alpha_u+\gamma\gamma_x}\leqslant\frac{1-\alpha_f}{\alpha_g}\frac{g_m^{min}}{f_m^{max}}\leqslant\frac{1-\alpha_f}{\alpha_g}\left|\frac{g_m\left(x_{j-1}\right)}{f_m\left(x_{j-1}\right)}\right|. \tag{64}$$

That fulfills the condition in (54). Thus, the proof is completed.

Remark 3. To acquire the parameters such as $\alpha_f,\alpha_g,f_m^{max}$ and g_m^{min}, the design engineers can determine it by their experience according to the controlled plant or monitoring the response which will be demonstrated by the section of numerical results.By considering SqvEIAR dynamics with the vaccination policy, it's obvious that the infected individual should be decreased by increasing the vaccination. Thus, in this case, the controlled plant has a negative control direction. Therefore, the analysis of Theorem 4.1 is extended by the following Lemma.

Lemma 4.1. *For the case of negative control direction of SqvEIAR dynamics (1) according to the impulsive vaccination $\upsilon(\kappa_j)$ (52), the closed-loop performance under Theorem 4.1 is still valid via the following condition:*

$$0<\frac{\alpha_f-1}{\alpha_g}\frac{g_m^{min}}{f_m^{max}}\leqslant\frac{\gamma\gamma_x}{\alpha_u+\gamma\gamma_x}\leqslant\frac{\alpha_f+1}{\alpha_g}\frac{g_m^{min}}{f_m^{max}}. \tag{65}$$

Proof. Let's define the Lyapunov function $\mathfrak{L}(j)$ as

$$\mathfrak{L}\left(j\right)=x^2\left(j\right). \tag{66}$$

Recalling dynamics in (55) and (58), the change of Lyapunov function $\Delta\mathfrak{L}(j)$ is derived as

$$\begin{aligned}\Delta\mathfrak{L}(j)=&\ x^2\left(j\right)-x^2\left(j-1\right),\\ =&\ \left[f_T\left(x_{j-1}\right)-\gamma_o\left(x_{j-1}\right)f_m\left(x_{j-1}\right)g_T\left(x_{j-1}\right)\right]^2-[x(j-1)]^2,\\ =&\ -2\gamma_o\left(x_{j-1}\right)f_m\left(x_{j-1}\right)f_T\left(x_{j-1}\right)g_T\left(x_{j-1}\right)+f_T^2\left(x_{j-1}\right)+\gamma_o^2\left(x_{j-1}\right)f_m^2\left(x_{j-1}\right)g_T^2\left(x_{j-1}\right)-x^2\left(j-1\right).\end{aligned} \tag{67}$$

According to the SqvEIAR dynamics in (1) and (11) and the equivalent model in (14), it's clear that $I(k)$ is always positive or $x(\kappa_j)\geqslant 0$ leading to

$f_m(x_{j-1})\geqslant 0$ and $f_T(x_{j-1})\geqslant 0$. Thereafter, by using (12) and (13), we obtain

$$\begin{aligned}\Delta\mathfrak{L}(j)\leqslant\ & 2\gamma_o\left(x_{j-1}\right)f_m\left(x_{j-1}\right)\alpha_f\alpha_g x^2\left(j-1\right)+\alpha_f^2x^2\left(j-1\right)+\alpha_g^2\gamma_o^2\left(x_{j-1}\right)f_m^2\left(x_{j-1}\right)x^2\left(j-1\right)-x^2\left(j-1\right),\\ \leqslant\ & \left[\alpha_f^2+2\gamma_o\left(x_{j-1}\right)f_m\left(x_{j-1}\right)\alpha_f\alpha_g+\alpha_g^2\gamma_o^2\left(x_{j-1}\right)f_m^2\left(x_{j-1}\right)-1\right]\times x^2\left(j-1\right),\\ \leqslant\ & \left[\left[\alpha_f+\alpha_g\gamma_o\left(x_{j-1}\right)f_m\left(x_{j-1}\right)\right]^2-1\right]x^2\left(j-1\right).\end{aligned}\tag{68}$$

For $\Delta\mathfrak{L}(j)\leq 0$, it's required that

$$-1\leqslant\alpha_f+\alpha_g\gamma_o\left(x_{j-1}\right)f_m\left(x_{j-1}\right)\leqslant 1,\tag{69}$$

or

$$-1\leqslant\alpha_f+\alpha_g\frac{\gamma\gamma_x g_m\left(x_{j-1}\right)f_m\left(x_{j-1}\right)}{\gamma_u+\gamma\gamma_x g_m^2\left(x_{j-1}\right)}\leqslant 1.\tag{70}$$

By using (53), thus, the relation in (70) is rearranged as

$$-1\leqslant\alpha_f+\alpha_g\frac{\gamma\gamma_x g_m\left(x_{j-1}\right)f_m\left(x_{j-1}\right)}{\left(\alpha_u+\gamma\gamma_x\right)g_m^2\left(x_{j-1}\right)}\leqslant 1,\tag{71}$$

or

$$-\frac{1+\alpha_f}{\alpha_g}\leqslant\frac{\gamma\gamma_x f_m\left(x_{j-1}\right)}{\left(\alpha_u+\gamma\gamma_x\right)g_m\left(x_{j-1}\right)}\leqslant\frac{1-\alpha_f}{\alpha_g}.\tag{72}$$

For the case of negative control direction, we have

$$g_m\left(x(\kappa_{j-1})\right)<0,\tag{73}$$

or

$$g_m\left(x_{j-1}\right)=-\left|g_m\left(x_{j-1}\right)\right|.\tag{74}$$

By using (74), the relation in (72) can be rearranged as

$$\frac{1+\alpha_f}{\alpha_g}\frac{\left|g_m\left(x_{j-1}\right)\right|}{f_m\left(x_{j-1}\right)}\geqslant\frac{\gamma\gamma_x}{\alpha_u+\gamma\gamma_x}\geqslant-\frac{1-\alpha_f}{\alpha_g}\frac{\left|g_m\left(x_{j-1}\right)\right|}{f_m\left(x_{j-1}\right)},\tag{75}$$

or

$$\frac{\alpha_f-1}{\alpha_g}\frac{\left|g_m\left(x_{j-1}\right)\right|}{f_m\left(x_{j-1}\right)}\leqslant\frac{\gamma\gamma_x}{\alpha_u+\gamma\gamma_x}\leqslant\frac{\alpha_f+1}{\alpha_g}\frac{\left|g_m\left(x_{j-1}\right)\right|}{f_m\left(x_{j-1}\right)}.\tag{76}$$

Thus, the relation in (76) is conclusively conducted as

Table 2
Initial and parameter values.

Parameters	Values	Parameters	Values
$S(1)$	8,000	e	0.7
$Q(1)$	0	ω	0.1
$V(1)$	0	p	0.1
$E(1)$	1,000	$\mathfrak{r}$	0.3
$I(1)$	500	α	0.3
$A(1)$	500	$\mathfrak{f}$	0.965
$N(1)$	10,000	$\mathfrak{n}$	0.3
$\mathfrak{z}$	0.02	λ	0.1
λ	0.1	ϵ_L	0
q_L	0.5	d_L	1

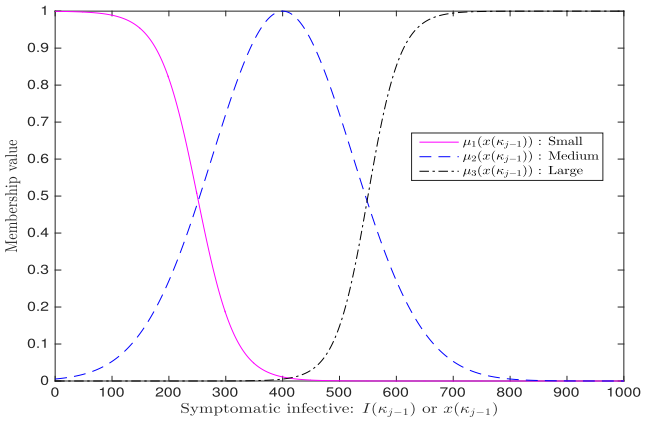

Fig. 4. Membership functions of $I(\kappa_{j-1})$ or $x(\kappa_{j-1})$..

$$\frac{\alpha_f-1}{\alpha_g}\frac{g_m^{min}}{f_m^{max}}\leqslant\frac{\gamma\gamma_x}{\alpha_u+\gamma\gamma_x}\leqslant\frac{\alpha_f+1}{\alpha_g}\frac{g_m^{min}}{f_m^{max}}.\tag{77}$$

The proof is completed.

Remark 4. The negative control direction of SqvEIAR dynamics under the proposed vaccination policy can be validated by the plot of $g_m(\kappa_j)$ in Fig. 7. The negative value of $g_m(\kappa_j)$ is obviously observed along with the

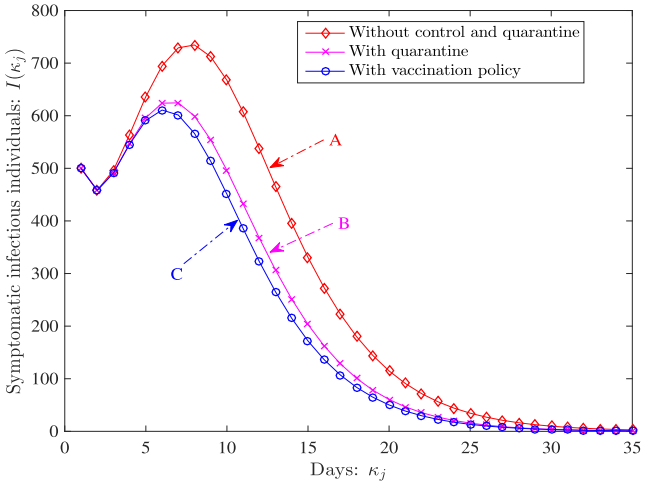

Fig. 5. Plots of symptomatic infectious $I(\kappa_j)$ populations.

operation.

Algorithm 1: Daily vaccination policy and inner-loop of equivalent model.

Input: $I(\kappa_j)$ or $x(\kappa_j)$: Daily sampling

Output: $u(\kappa_j)$ or $v(\kappa_j)$: Daily vaccination policy

Data: Membership function μ_l for $l = 1, 2, 3$, Model's parameters, Controller's parameters, $\beta_f(\kappa_{j-1}, 0)$, $\beta_g(\kappa_{j-1}, 0)$, $u(\kappa_{j-1})$ and $x(\kappa_{j-1})$.

Determine $\phi(\kappa_{j-1}, i)$ in (19) and $\hat{e}(\kappa_j, 1)$ by setting $i = 0$.

Keep $\phi(\kappa_{j-1}, 0)$ constant as $\phi(\kappa_{j-1})$.

for $i \geq i_{max}$ *or* $|\hat{e}(\kappa_j, i+1)| \leq \varepsilon_o$ **do**

  Determine $\hat{x}(\kappa_j, i+1)$ by (19).

  Determine $\hat{e}(\kappa_j, i+1)$ by (18).

  Update $\beta_f(\kappa_{j-1}, i+1)$ and $\beta_g(\kappa_{j-1}, i+1)$ by (23) and (26), respectively.

  Set $i := i + 1$.

Set $f_m(x(j-1)) = \beta_f^T(\kappa_{j-1}, i_{final})\phi(\kappa_{j-1})$ and $g_m(x(j-1)) = \beta_g^T(\kappa_{j-1}, i_{final})\phi(\kappa_{j-1})$.

if *Condition (65) = True* **then**

  Determine $u(\kappa_j)$ by (52).

else if $j \geq 2$ **then**

  Recall $f_m(x(j-2))$ and $g_m(x(j-2))$ and determine $u(\kappa_j)$.

else

  Recall $f_m(x(j-1))$ and $g_m(x(j-1))$ from the previous iteration and determine $u(\kappa_j)$.

For the conclusion, the Algorithm 1 is given to represent the learning laws for the equivalent model and the determination of the proposed vaccination policy according to the condition (65) of Lemma 4.1.

5. Controller setting and numerical results

In this section, the design of the proposed scheme is demonstrated and the validation results are given by the numerical system of SqvEIAR dynamics (1) altogether with impulsive traveling of individuals.

5.1. Parameters design and setting

Table 2 represents all parameter values of SqvEIAR dynamics in (1) and initial values. Fig. 4 illustrates the membership functions μ of FREN

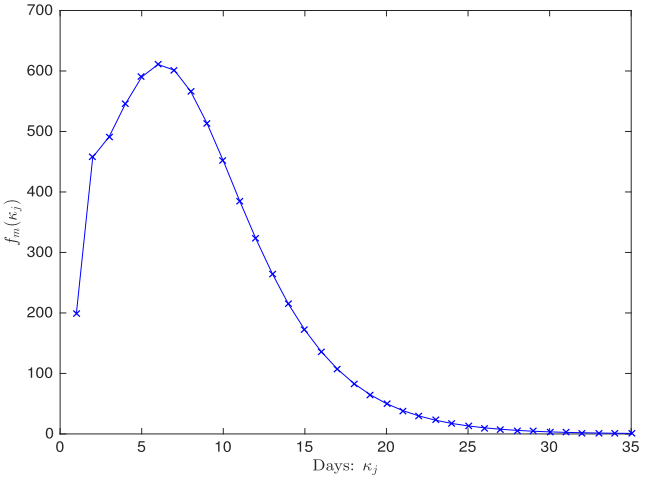

Fig. 6. Estimated function $f_m(\kappa_j)$.

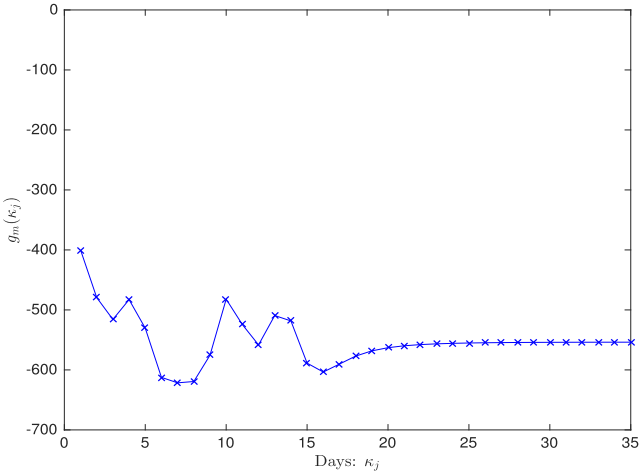

Fig. 7. Estimated function $g_m(\kappa_j)$.

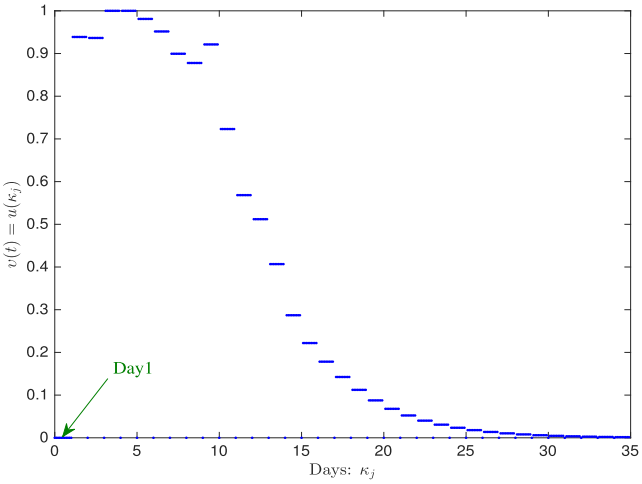

Fig. 8. Vaccination policy $u(\kappa_j)$.

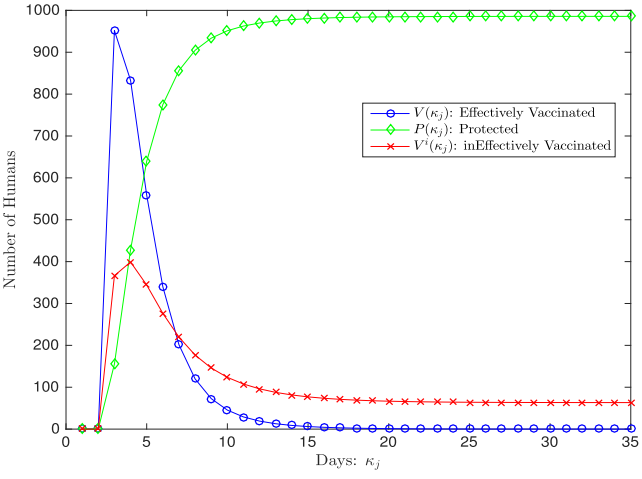

Fig. 9. Vaccinated individuals.

in Fig. 3 when $N = 3$ and $I(\kappa_{j-1})$ or $x(\kappa_{j-1}) \in [0, 1000]$. It's worth to denote that, in this work, the setting of the range of $x(\kappa_{j-1})$ is double of $I(1)$ in Table 2.

The vaccination policy is in the range of [0,1]. Thus, the parameter u_M is given as $u_M = \max(v) = 1$. With 3 membership functions, we have

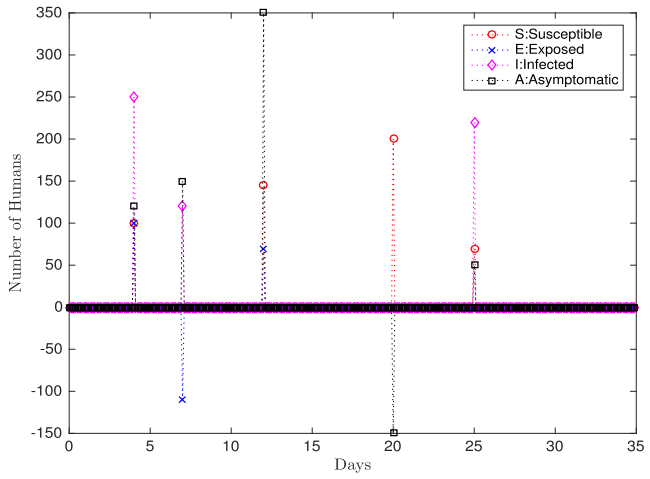

Fig. 10. Impulsive immigrating pattern.

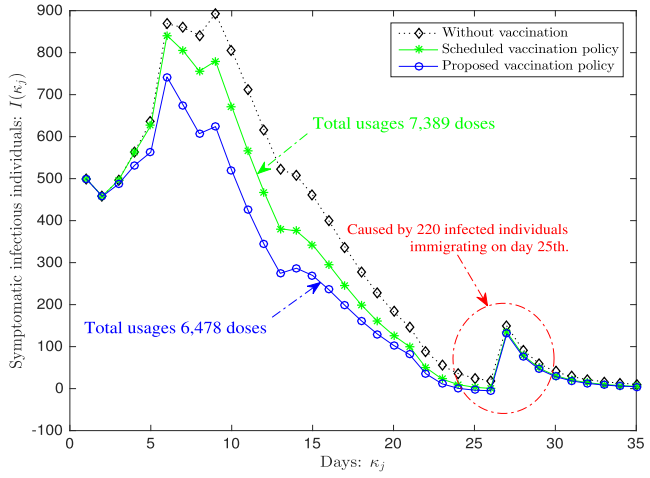

Fig. 11. Symptomatic infectious $I(\kappa_j)$ with Impulsive immigrating..

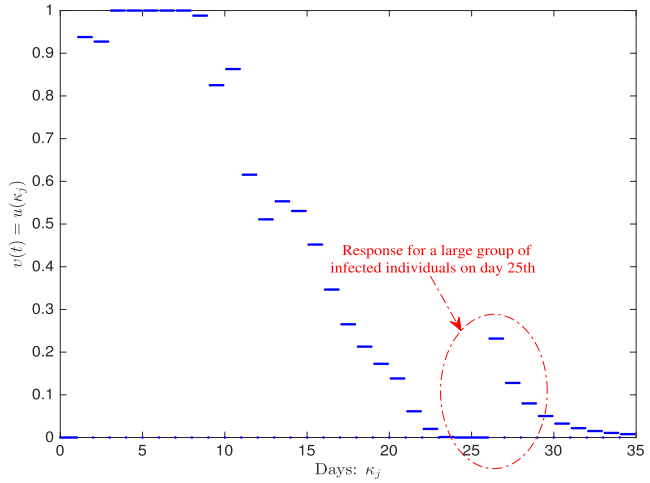

Fig. 12. Vaccination policy $u(\kappa_j)$ with Impulsive immigrating..

$\phi_M = 3$. By recalling the results from Theorem 3.1 where $\gamma_f = 0.7$ and $\gamma_g = 0.7$, thus, the learning rates for β_f and β_g can be determined as

$$0 \leqslant \eta_f < \frac{\gamma_f}{\phi_M} = \frac{0.7}{3} = 0.2333, \tag{78}$$

and

$$0 \leqslant \eta_g < \frac{\gamma_g}{u_M^2 \phi_M} = \frac{0.7}{1 \times 3} = 0.2333, \tag{79}$$

respectively. In this work, we select $\eta_f = 0.2$ and $\eta_g = 0.2$.

Thereafter, the parameters of the controller are designed according to Theorem 4.1 and Lemma 4.1. The sampling time k is given as $T_s = 0.001$ [day] in this simulation. Let's simply select $g_m^{min} = 200, f_m^{max} = 700, \alpha_f = 0.7$ and $\alpha_g = 0.7$. It yields $\gamma = 0.7, \gamma_x = 0.5$ and $\alpha_u = 0.25$ such that

$$\frac{\gamma\gamma_x}{\alpha_u + \gamma\gamma_x} = 0.5833 \leqslant \frac{\alpha_f + 1}{\alpha_g} \frac{g_m^{min}}{f_m^{max}} = 0.6939. \tag{80}$$

Thus, the condition in Lemma 4.1 has been fulfilled.

5.2. Validation results

By testing SqvEIAR dynamics (1) without applying the controller ($\upsilon(t) = 0$) and quarantine ($\lambda = 0$), the population of symptomatic infectious individuals $I(\kappa_j)$ is depicted by the A-plot in Fig. 5. Next, the parameter λ is give as $\lambda = 0.5$ for quarantining. Thus, the population of $I(\kappa_j)$ is shown by the B-plot in Fig. 5. Thereafter, the C-plot in Fig. 5 represents $I(\kappa_j)$ of SqvEIAR dynamics when applying only the vaccination policy as $\upsilon(t) = u(\kappa_j)$ in (52) and $\lambda = 0$. It's obvious that the peak of symptomatic infectious individuals is definitely reduced.

Fig. 6 displays the plot of $f_m(\kappa_j)$. It's clear that the setting as $f_m^{max} = 700$ in Section 5.1 has been validated. The plot of $g_m(\kappa_j)$ is illustrated in Fig. 7. It proves the case of negative control direction regarding to the establishment of Lemma 4.1. Furthermore, it can be observed $|g_m(\kappa_j)|_{min} = 400$. Thus, the setting as $g_m^{min} = 200$ in Section 5.1 has been also validated. The vaccination policy is represented by the plot in Fig. 8 and the details are fully illustrated by Fig. 9.

5.3. Results with impulsive traveling and migrating

The effects of impulsive immigrating and traveling are considered in this test. Fig. 10 presents the impulsive moving pattern which contains four groups such that $S(\kappa_j), E(\kappa_j), I(\kappa_j)$ and $A(\kappa_j)$. It's worth emphasizing that those varying individuals are assumed to be unknown. Thus, the controller generates the vaccination policy $\upsilon(t)$ by using the equivalent model only.

To demonstrate the performance of the proposed vaccination policy, the scheduling vaccination policy [18] is firstly utilized with $\upsilon(t) = 0.7$ along 4 weeks (28 days). Thereafter, the proposed scheme is employed by using the same setting in Section 5.1. Fig. 11 illustrates the plots of $I(\kappa_j)$ with difference vaccination policies. The result of no vaccination is firstly considered with the higher number of symptomatic infectious individuals. Afterward, the scheduling vaccination is employed. It's clear that the number of symptomatic infectious individuals is significantly decreased and 7,389 doses of vaccine are used. Finally, the proposed vaccination policy is utilized. Only 6,478 doses of vaccine are used but the number of symptomatic infectious individuals is obviously reduced according to the result from the scheduling vaccination. Furthermore, the proposed vaccination policy is represented by the plot in Fig. 12. After day 23^{rd}, the vaccination policy is reached zero because the epidemic is under control. On day 25^{th}, it has large immigrating amount of $I(\kappa_j = 25)$. Thus, the vaccination policy is spontaneously increased. That will suggest the authorities gaining control of the epidemic.

6. Conclusions

In this paper, the optimal vaccinated strategy has been derived by using only the daily data of symptomatic infectious individuals and

considering the impulsive immigrants of susceptible, exposed, symptomatic infectious and asymptomatic infectious individuals. SqvEIAR dynamics have been developed to accomplish the vaccination's effectiveness, antiviral factor and quarantine. By utilizing only the daily data of symptomatic infectious individuals the equivalent model has been established with the impulsive axis. Therefore, the negative control direction of the controlled SqvEIAR dynamics with the vaccination policy has been validated by the negative value of the estimated function $g_m(\kappa_j)$. By employing the proposed vaccination policy, the number of symptomatic infectious individuals has been significantly reduced with the fewer usage vaccines. Furthermore, the adaptive algorithm has validated the fast response according to the impulsive traveling and migrating of individuals.

The optimal vaccination proposed in this work may provide a feasible non-pharmaceutical policy for the authority to control the COVID-19 epidemic. Currently, the vaccines are all in the intensively developing phase and the new variants of the coronavirus are persistently discovered thus the new or updated data will be included to enchant the performance as our upcoming future work.

CRediT authorship contribution statement

C. Treesatayapun: Conceptualization, Methodology, Software, Data curation, Visualization, Investigation, Writing - original draft, Writing - review & editing.

Declaration of Competing Interest

The authors declare that they have no known competing financial interests or personal relationships that could have appeared to influence the work reported in this paper.

Acknowledgment

This work has been supported by Mexican Research Organization CONACyT grant# 257253.

References

[1] Worldometers, Worldometers coronavirus; 2021. https://www.worldometers.info/coronavirus/, [Accessed 08-15-2021].
[2] M. Adrian, A. Zegarra, S.D. Infante, D.B. Carrasco, D.O. Liceaga, COVID-19 optimal vaccination policies: A modeling study on efficacy, natural and vaccine-induced immunity responses, Mathematical Biosciences 337 (2021), 108614.
[3] Ourworldindata, Coronavirus (COVID-19) Vaccinations; 2021. https://ourworldindata.org/covid-vaccinations, [Accessed 08-17-2021].
[4] P.D. Giamberardino, D. Iacoviello, Evaluation of the effect of different policies in the containment of epidemic spreads for the COVID-19 case, Biomedical Signal Processing and Control 65 (2021), 102325.
[5] H. Aghdaoui, A.L. Alaoui, K.S. Nisar, M. Tilioua, On analysis and optimal control of a SEIRI epidemic model with general incidence rate, Results in Physics 20 (2021), 103681.
[6] L. Leonardo, R. Xavier, A modified SEIR model to predict the COVID-19 outbreak in Spain and Italy: Simulating control scenarios and multi-scale epidemics, Results in Physics 21 (2021), 103746.
[7] M. Mandal, S. Jana, S.K. Nandi, A. Khatua, S. Adak, T.K. Kar, A model based study on the dynamics of COVID-19: Prediction and control, Chaos Solitons Fractals 136 (2020), 109889.
[8] H. Khan, R.N. Mohapatra, K. Vajravelu, S.J. Liao, The explicit series solution of SIR and SIS epidemic models, Applied Mathematics and Computation 215 (2) (2009) 653–659.
[9] M.D. la Sen, S. Alonso-Quesada, Vaccination strategies based on feedback control techniques for a general SEIR- epidemic model, Applied Mathematics and Computation 218 (7) (2011) 3888–3904.
[10] P.J.I. Ellis, Modelling suggests ABO histo-incompatibility may substantially reduce SARS-CoV-2 transmission, Epidemics 35 (2021), 100446.
[11] R. Padmanabhan, N. Meskin, T. Khattab, M. Shraim, M. Al-Hitmia, Reinforcement learning-based decision support system for COVID-19, Biomedical Signal Processing and Control 68 (2021), 102676.
[12] J. Stehle, N. Voirin, A. Barrat, C. Cattuto, V. Colizza, L. Isella, C. Regis, J.F. Pinton, N. Khanafer, W.V. d. Broeck and P. Vanhem, "Simulation of an SEIR infectious disease model on the dynamic contact network of conference attendees," BMC Medicine, vol. 9, no. 87, p. 1–15, 2011.
[13] J. Andrade, J. Duggan, An evaluation of Hamiltonian Monte Carlo performance to calibrate age-structured compartmental SEIR models to incidence data, Epidemics 33 (2020), 100415.
[14] M.A. Hadi, H.I. Ali, Control of COVID-19 system using a novel nonlinear robust control algorithm, Biomedical Signal Processing and Control 64 (2021), 102317.
[15] Y.K. Xie, Z. Wang, J.W. Lu, Y.X. Li, Stability analysis and control strategies for a new SIS epidemic model in heterogeneous networks, Applied Mathematics and Computation 383 (2020), 125381.
[16] M.A. Hadi, Z.M. Amean, New strategy to control covid-19 pandemic using lead/lag compensator, Biomedical Signal Processing and Control 68 (2021), 102669.
[17] N.P. Dong, H.V. Long, A. Khastan, Optimal control of a fractional order model for granular SEIR epidemic with uncertainty, Commun Nonlinear Sci Numer Simulat 88 (2020), 105312.
[18] I. Al-Darabsah, Threshold dynamics of a time-delayed epidemic model for continuous imperfect-vaccine with a generalized nonmonotone incidence rate, Nonlinear Dynamics 101 (2020) 1281–1300.
[19] N. Sebastian, F.A. Inthamoussou, F. Valenciaga, H.D. Battista, F. Garelli, Potentials of constrained sliding mode control as an intervention guide to manage COVID19 spread, Biomedical Signal Processing and Control 67 (2021), 102557.
[20] R. Abolpour, S. Siamak, M. Mohammadi, P. Moradi, M. Dehghani, Linear parameter varying model of COVID-19 pandemic exploiting basis functions, Biomedical Signal Processing and Control 70 (2021), 102999.
[21] C. Zhan, J. Chen, H. Zhang, An investigation of testing capacity for evaluating and modeling the spread of coronavirus disease, Information Sciences 561 (2021) 211–229.
[22] A. Rajaei, M. Raeiszadeh, V. Azimi, M. Sharifi, State estimation-based control of COVID-19 epidemic before and after vaccine development, Journal of Process Control 102 (2021) 1–4.
[23] B. Peddinti, A. Shaikh, K.R. Bhavya, K.C. Nithin-Kumar, Framework for Real-Time Detection and Identification of possible patients of COVID-19 at public places, Biomedical Signal Processing and Control 68 (2021), 102605.
[24] L. Xue, S. Jing, J.C. Miller, W. Suna, H. Li, J.G. Estrada-Francoc, J.M. Hyman, H. Zhue, A data-driven network model for the emerging COVID-19 epidemics in Wuhan, Toronto and Italy, Mathematical Biosciences 326 (2020), 108391.
[25] N.Y. Khanday and S.A. Sofi, "Deep Insight: Convolutional Neural Network and its Applications for COVID-19 Prognosis," Biomedical Signal Processing and Control, vol. In Press, p. 102814, 2021.
[26] Z. Abbasi, I. Zamani, A.H. Amiri-Mehra, M. Shafieirad, A. Ibeas, Optimal Control Design of Impulsive SQEIAR Epidemic Models with Application to COVID-19, Chaos, Solitons and Fractals 139 (2020), 110054.
[27] M.P. Hossain, A. Junus, X. Zhu, P. Jia, T. Wen, D. Pfeiffer, H. Yuan, The effects of border control and quarantine measures on the spread of COVID-19, Epidemics 32 (2020), 100397.
[28] M.F. Villa-Tamayo, P.S. Rivadeneira, Adaptive Impulsive Offset-Free MPC to Handle Parameter Variations for Type 1 Diabetes Treatment, Industrial & Engineering Chemistry Research 59 (2020) 5865–5876.
[29] G. Hernandez-Mejia, X. Du, A.Y. Alanis, E.A. Hernandez-Vargas, Bounded input impulsive control for scheduling therapies, Journal of Process Control 102 (2021) 34–43.
[30] M. Bachar, J.G. Raimann, P. Kotanko, Impulsive mathematical modeling of ascorbic acid metabolism in healthy subjects, Journal of Theoretical Biology 392 (2016) 35–47.
[31] Y. Gao, X. Zhang, G. Lu, Y. Zheng, Impulsive synchronization of discrete-time chaotic systems under communication constraints, Commun. Nonlinear Sci. Numer. Simul. 16 (2011) 1580–1588.
[32] X. Liguang, S.G. Shuzhi, Set-stabilization of discrete chaotic systems via impulsive control, Applied Mathematics Letters 53 (2016) 52–62.
[33] L.F. Nie, Z.D. Teng, Effects of impulsive control on permanence and extinction of lactic acid fermentation, Journal of Process Control 24 (7) (2014) 1121–1134.
[34] D. He, L. Xu, Ultimate boundedness of non-autonomous dynamical complex networks under impulsive control, IEEE Trans. Circuits Syst. II 62 (2015) 997–1001.
[35] F. Cacace, V. Cusimano, P. Palumbo, Optimal impulsive control with application to antiangiogenic tumor therapy, IEEE Trans. Control Syst. Technol. 28 (1) (2020) 106–117.
[36] Q. Wei, R. Song, Z. Liao, B. Li, F.L. Lewis, Discrete-time impulsive adaptive dynamic programming, IEEE Trans. Cybern. 50 (10) (2020) 4293–4306.
[37] G. Hernandez-Mejia, A.Y. Alanis, E.A. Hernandez-Vargas, Neural inverse optimal control for discrete-time impulsive systems, Neurocomputing 314 (2018) 101–108.
[38] L.O. Naraigh, A. Byrne, Piecewise-constant optimal control strategies for controlling the outbreak of COVID-19 in the Irish population, Mathematical Biosciences 330 (2020), 108496.
[39] M.O. Berner, V. Scherer, M. Monnigmann, Controllability analysis and optimal control of biomass drying with reduced order models, Journal of Process Control 89 (2020) 1–10.
[40] W. Jianfang, H. Ruo, L. Ming, L. Shanshan, Z. Xizheng, H. Jun, C. Jiaxu, L. Xiangjun, Diagnosis of sleep disorders in traditional Chinese medicine based on

adaptive neuro-fuzzy inference system, Biomedical Signal Processing and Control 70 (2021), 102942.
[41] G. Hernandez-Mejia, A.Y. Alanis, M. Hernandez-Gonzalez, R. Findeisen, E. A. Hernandez-Vargas, Passivity-based inverse optimal impulsive control for influenza treatment in the host, IEEE Trans. Control Syst. Technol. 28 (1) (2020) 94–105.
[42] C. Treesatayapun, S. Uatrongjit, Adaptive controller with Fuzzy rules emulated structure and its applications, Engineering Applications of Artificial Intelligence 18 (2005) 603–615.
[43] C. Treesatayapun, Prescribed performance of discrete-time controller based on the dynamic equivalent data model, Applied Mathematical Modelling 78 (2020) 366–382.
[44] Z. Hou, R. Chi, H. Gao, An overview of dynamic-linearization-based data-driven control and applications, IEEE Trans. Ind. Electron. 64 (5) (2017) 4076–4090.
[45] C. Treesatayapun, Discrete-time adaptive controller based on non-switch reaching condition and compact system dynamic estimator, J. Franklin I. 354 (5) (2017) 6783–6804.
[46] X. Liguang, G. Shuzhi-Sam, Set–stabilization of discrete chaotic systems via impulsive control, Applied Mathematics Letters 53 (2016) 52–62.